

Kv7.1 ion channels require a lipid to couple voltage sensing to pore opening

Mark A. Zayzman^a, Jonathan R. Silva^a, Kelli Delaloye^a, Yang Li^a, Hongwu Liang^a, H. Peter Larsson^b, Jingyi Shi^a, and Jianmin Cui^{a,1}

^aDepartment of Biomedical Engineering, Center for the Investigation of Membrane Excitability Diseases, Cardiac Bioelectricity and Arrhythmia Center, Washington University in St. Louis, St. Louis, MO 63130-4862; and ^bDepartment of Physiology and Biophysics, Miller School of Medicine, University of Miami, Miami, FL 33136-1015

Edited by Richard W. Aldrich, University of Texas at Austin, Austin, TX, and approved June 14, 2013 (received for review March 26, 2013)

Voltage-gated ion channels generate dynamic ionic currents that are vital to the physiological functions of many tissues. These proteins contain separate voltage-sensing domains, which detect changes in transmembrane voltage, and pore domains, which conduct ions. Coupling of voltage sensing and pore opening is critical to the channel function and has been modeled as a protein–protein interaction between the two domains. Here, we show that coupling in Kv7.1 channels requires the lipid phosphatidylinositol 4,5-bisphosphate (PIP₂). We found that voltage-sensing domain activation failed to open the pore in the absence of PIP₂. This result is due to loss of coupling because PIP₂ was also required for pore opening to affect voltage-sensing domain activation. We identified a critical site for PIP₂-dependent coupling at the interface between the voltage-sensing domain and the pore domain. This site is actually a conserved lipid-binding site among different K⁺ channels, suggesting that lipids play an important role in coupling in many ion channels.

channelopathy | electromechanical coupling | KCNQ | voltage channel | phosphoinositide

Voltage-gated ion channels are integral membrane proteins that sense membrane voltage and respond by opening or closing a transmembrane pore. Ionic currents carried by voltage-gated ion channels control contraction in muscle, encode information in the nervous system, and trigger secretion in neurohormonal tissues. Voltage-gated ion channels contain four voltage-sensing domains (VSDs) and a central pore domain (PD) that are structurally distinct (1, 2). In voltage-gated potassium (Kv) channels, the first four transmembrane segments (S1–S4) of each α -subunit forms a VSD. In response to changes in transmembrane voltage, the VSD undergoes a conformational change, called activation, during which membrane depolarization moves the S4 segment outward (3). The PD is formed by the last two transmembrane segments (S5, S6) from four α -subunits and undergoes a mainly voltage-independent conformational change during which the intracellular ends of the S6 segments bend, opening the ionic pore (4, 5). Interestingly, the PD and VSD can exist in pore-only (6) and voltage sensor-only proteins, respectively, where they function independently (7, 8). Confining sensitivity to voltage, or to other stimuli, within a domain diversifies the ion channel properties that can be achieved by partnering different pore and sensor domains. However, this modular architecture also raises a fundamental question as to how VSD activation is transmitted to the PD. Previous studies of this coupling process have revealed the importance of direct protein–protein interactions at the VSD–PD interface (9–13); however, the possible role of membrane lipids in VSD–PD coupling remains undetermined.

The membrane lipid phosphatidylinositol 4,5-bisphosphate (PIP₂) modulates the activity of many ion channels, including some voltage-gated channels (14). Notably, all members of the Kv7 family (Kv7.1–Kv7.5), which play important physiological roles in the cardiac (15) or the nervous (16) systems, require PIP₂ to be opened by membrane depolarization (17). In fact, silencing

of Kv7 channels by PIP₂ depletion is known to underlie the modulation of neuronal excitability by hormone receptor signaling (16). Despite this relevance to human health, it remains unclear where PIP₂ binds and why PIP₂ binding is required for voltage-dependent gating. We sought to determine, in Kv7.1 channels, whether PIP₂ is required for any of three fundamental gating processes: activation of the VSD by membrane depolarization, coupling of VSD activation and PD opening, or opening of the PD to allow passage of ions.

Results

PIP₂ Is Not Required for VSD Activation. Using voltage-clamp fluorometry on channels expressed in *Xenopus oocytes*, we determined the effect of PIP₂ depletion on VSD activation and PD opening simultaneously. In voltage-clamp fluorometry, fluorescent labeling of the S3–S4 linker generates measurable changes in fluorescence intensity that are correlated with S4 movement during VSD activation; meanwhile, measurement of the whole-cell ionic current detects PD opening (Fig. 1A) (18). As reported previously, we used pseudo-wild-type (psWT)—C214A/G219C/C331A—Kv7.1 channels to avoid nonspecific labeling of native Cys214 and Cys331 and labeled position G219C with Alexa 488 C5 maleimide (19). To deplete PIP₂, we expressed the voltage-sensing phosphatase from *Ciona intestinalis* (CiVSP), a lipid phosphatase that rapidly dephosphorylates PIP₂ upon membrane depolarization (20, 21). When we activated CiVSP with a train of six depolarizing (+60-mV) pulses (Fig. 1B), the psWT channel current amplitude was dynamically and severely decreased within the first pulse to only $18 \pm 2\%$ that of oocytes expressing psWT channels alone and recorded on the same day. Application of five subsequent pulses produced yet further inhibition (−CiVSP: $I_6/I_1 = 88 \pm 1\%$; +CiVSP: $I_6/I_1 = 31 \pm 2\%$; $P < 0.0001$) leaving only $4 \pm 3\%$ of the current amplitude in the same day controls (Fig. 1C). In clear contrast, CiVSP activation did not decrease the magnitude of the fluorescence signal change ($\Delta F/F$) during the first pulse or upon subsequent pulses (−CiVSP: $\Delta F_6/\Delta F_1 = 88 \pm 1\%$; +CiVSP: $\Delta F_6/\Delta F_1 = 86 \pm 1\%$; $P = 0.246$; Fig. 1C), indicating that VSD activation still occurs after PIP₂ depletion. As an alternative method to voltage-clamp fluorometry we detected VSD activation using 2-sulfo-natoethyl methanethiosulfonate (MTSES) modification of I230C in S4, which is only accessible to MTSES when the VSD is activated (3, 22) (Figs. S1–S3). This experiment confirmed that VSD activation occurs in the absence of PIP₂. After PIP₂ depletion, we found

Author contributions: M.A.Z., J.R.S., H.P.L., and J.C. designed research; K.D. and J.S. generated mutant channels; M.A.Z., K.D., Y.L., and H.L. performed research; Y.L. collected data in Fig. 4D; H.L. collected part of data in Fig. 5C; M.A.Z. analyzed data; and M.A.Z., J.R.S., H.P.L., J.S., and J.C. wrote the paper.

The authors declare no conflict of interest.

This article is a PNAS Direct Submission.

¹To whom correspondence should be addressed. E-mail: jcui@wustl.edu.

This article contains supporting information online at www.pnas.org/lookup/suppl/doi:10.1073/pnas.1305167110.

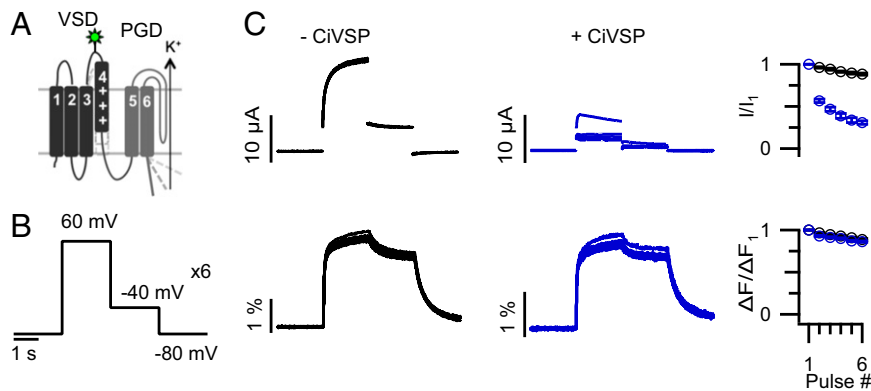


Fig. 1. PIP_2 depletion suppresses pore opening but not VSD activation. (A) Cartoon of channel motions measured by voltage-clamp fluorometry. (B) Voltage protocol. (C) Ionic currents (Upper) and relative fluorescent intensity changes ($\Delta F/F$; Lower) from cells expressing psWT Kv7.1 alone (black) or with CiVSP (blue). Example raw data traces (Left, Center). Average value at the end of each 60-mV pulse normalized to that at the first pulse (Right). Error bars represent SEM and $n = 3\text{--}20$ for all figures.

that the steady-state voltage dependence of VSD activation, reflected in the fluorescence–voltage (F – V) relationship, was unchanged (Fig. S4 A–H), whereas the ionic currents were inhibited. Of note, the kinetics of the fluorescence signal changes did show a mild dependence on PIP_2 (Fig. S4 E, F, and I). Altogether, these results demonstrate that PIP_2 is not required for detection of membrane voltage within the VSD.

PIP2 Is Required for Coupling. We tested whether PIP_2 is required for coupling. Coupling can be quantified by measuring the effect of VSD activation on PD opening or by measuring how PD opening affects VSD activation (23, 24). We chose the latter approach because we could still measure VSD activation after PIP_2 depletion when PD opening became undetectable (Fig. 1). To promote pore opening, we introduced the mutation L353K into the S6 gate (25). Leu353 is located near the putative bundle crossing, and previous studies have shown that introduction of a positive or negative amino acid at this position results in a channel that remains open (25) as if the mutual electrostatic repulsion among the introduced charges destabilizes the closed state of the PD. psWT/L353K channels conducted instantaneous current at every voltage

we applied (Fig. 2 A and C), and these currents were not inhibited when we expressed and activated CiVSP with a train of six depolarizing pulses (+CiVSP: $I_6/I_1 = 102 \pm 2.4\%$; –CiVSP: $I_6/I_1 = 99 \pm 0.7\%$; $P = 0.185$; Fig. 2A). Furthermore, psWT/L353K currents reversed near the K^+ equilibrium (Fig. 2C) and were reduced when we applied the Kv7.1 pore blocker chromanol 293B (26) (Fig. 2B), providing evidence that the observed constitutive currents were indeed conducted by expressed psWT/L353K channels. By comparing the VSD activation of psWT and locked open psWT/L353K channels, we were able to detect VSD–PD coupling directly as a mild, but statistically significant ($P < 0.0001$), leftward shift in the F – V relationship (psWT/L353K: $V_{1/2} = -72.1 \pm 1.5$ mV; psWT: $V_{1/2} = -57.1 \pm 0.8$ mV; Fig. 2C, Left). This shift is consistent with the positive coupling between VSD activation and PD opening, i.e., less energy is required to activate the VSD if the PD is open. This shift is similar in magnitude to that observed in other channels locked open using metal bridging (24). When we depleted PIP_2 , using CiVSP, the psWT/L353K channels remained open, but their F – V relationship no longer differed ($P = 0.117$) from psWT channels (psWT + CiVSP: $V_{1/2} = -60.4 \pm 0.6$ mV; psWT/L353K + CiVSP: $V_{1/2} = -58.5 \pm 1.1$ mV; Fig. 2C, Right). This result indicates that PIP_2 is required for PD opening (by L353K) to promote VSD activation. We tested whether other mutations also require PIP_2 to affect VSD activation and identified two such mutations (S349A, G350A) (Fig. S5). Ser349, Gly350, and Leu353 are located in the S6 gate, and homology modeling predicted that they do not interact with the VSD or the S4–S5 linker (Fig. S5E). This is consistent with the idea that these mutations directly alter PD opening and indirectly affect VSD activation through PIP_2 -dependent coupling. Thus, our experiments show that PIP_2 is required both for VSD activation to cause PD opening (Fig. 1) and for PD opening to affect the activation of the VSD (Fig. 2). These findings show that a membrane lipid can be required for the functional coupling between the VSD and the PD.

We devised an equilibrium model of Kv7.1 gating by PIP_2 and voltage in which bound PIP_2 couples VSD and PD so that VSD activation enhances PD opening by a factor θ , and vice versa (Fig. 3A, Fig. S6, and *SI Materials and Methods* for full model derivation and fitting parameters). Our data regarding the voltage and PIP_2 dependence of the ionic current and VSD activation were fit well with this model (Fig. 3 B and C). The model does not include any direct effects of PIP_2 on the opening of the PD or the activation of the VSD, thus demonstrating that the requirement of PIP_2 for VSD–PD coupling alone is sufficient to quantitatively recapitulate the channel behavior. However, the possibility that PIP_2 may also have a minor direct effect on the opening of the PD cannot be excluded. Importantly, as observed

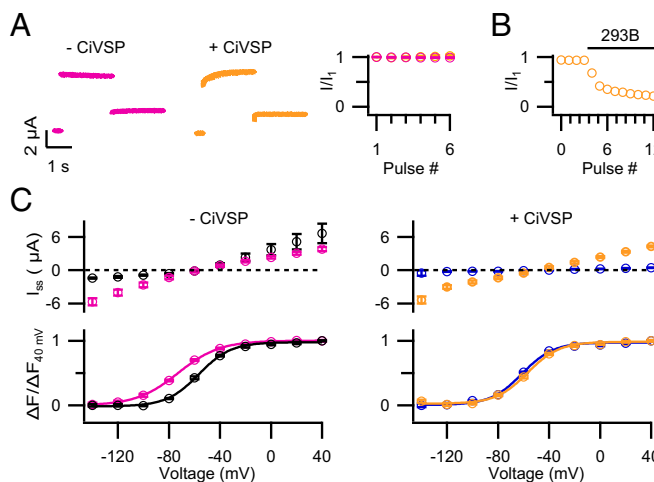


Fig. 2. VSD–PD coupling requires PIP_2 . Voltage-clamp fluorometry of psWT (black), psWT + CiVSP (blue), psWT/L353K (magenta), and psWT/L353K + CiVSP (orange). (A) Raw currents and normalized current amplitude as in Fig. 1. (B) Inhibition of current by 200 μM Chromanol 293B. (C) Steady-state current–voltage (Upper) and fluorescence–voltage (F – V) (Lower) relationships. For details of voltage protocol, see Fig. S4.

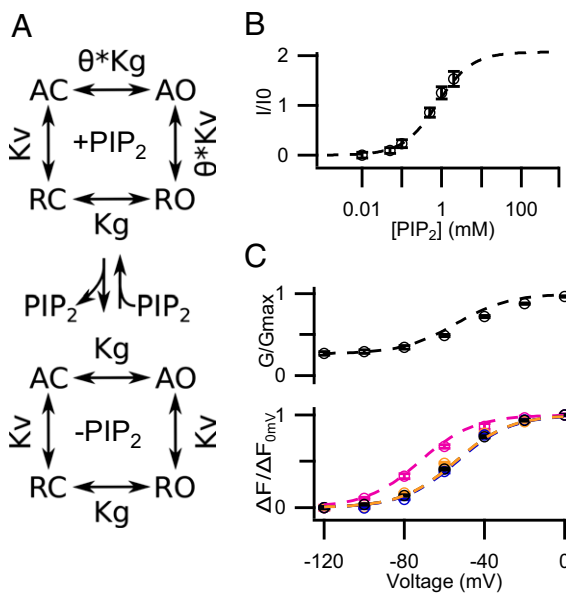


Fig. 3. Model of PIP₂-mediated coupling predicts observed gating behavior. (A) An equilibrium model of PIP₂- and voltage-dependent gating (Fig. S6 and SI Materials and Methods) used to fit (dotted lines) (B) the PIP₂-response curve of WT channels (data from ref. 32) and (C) the conductance–voltage (G – V ; Upper) and F – V relationships (Lower) of psWT (black), psWT + CiVSP (blue), psWT/L353K (magenta), and psWT/L353K + CiVSP (orange). Symbols represent experimental data. In the model, θ represents the coupling, whereas K_V and K_g describe the voltage sensor activation and pore opening, respectively, in the absence of PIP₂.

in our experiments, the model simulation predicted that PIP₂ depletion would not generate a measurable shift in the psWT F – V . This occurs because the intrinsic open probability of the PD is low and the coupling is weak, as indicated by several recent papers (27, 28).

PIP₂ Binds at the VSD–PD Interface. A critical step to understanding how PIP₂ binding mediates VSD–PD coupling is to identify its binding site. The most intuitive location is at the VSD–PD interface, a region that has already been shown to contain protein–

protein interactions important for Kv channel coupling (9–13). PIP₂ binding sites in proteins generally contain multiple basic residues located near the intracellular leaflet of the membrane to interact electrostatically with the negatively charged PIP₂ head group (29). Accordingly, using a Kv7.1 homology model, we identified 16 basic residues that are located near VSD–PD interface (30). These residues are highly conserved among the Kv7 channels, which require PIP₂ for voltage-dependent gating (17), but are poorly conserved among other Kv channels that do not require PIP₂ (31) (Fig. 4A). Using site-directed mutagenesis, we individually neutralized each of these basic residues in WT Kv7.1 and measured the effect on the expressed current amplitude, using two-electrode voltage clamp. Because the endogenous level of PIP₂ in the oocyte membrane is within the sensitive range of Kv7.1 (32), we expected that a mutation that disrupts PIP₂ binding would decrease the current. Indeed, we found that eight mutations (R190Q, R195Q, H258N, R259Q, K354N, R360Q, H363N, R366Q) severely decreased (>50% reduction; Fig. 4B and C, blue) the whole-cell current amplitude, and four mutations (R192Q, R243Q, K358N, K362N) had a milder reduction (<50% reduction; Fig. 4B and C, green). However, four neutralizing mutations (R181Q, K183N, K196N, R249Q; Fig. 4B and C, red) and three additional charge-reversing mutations (R249E, K358E, R360E; Fig. S7) actually increased the current amplitude. Importantly, we detected robust surface expression of the loss-of-current mutants by Western blot analysis of proteins labeled by extracellular biotin (Fig. 4D). This result shows that loss of current expression is not due to reduced protein synthesis or membrane trafficking. Furthermore, we detected fluorescent signal changes using voltage-clamp fluorometry for all of the loss-of-current mutations (Fig. 4E), indicating that these mutant channels not only expressed to the membrane but also retained VSD activation. Therefore, the loss-of-current mutations affected channel gating by decreasing coupling, consistent with decreased PIP₂ binding, or by decreasing PD opening.

We tested whether our mutations affected current amplitude by changing the apparent PIP₂ affinity. We measured the time course of the current rundown that occurs spontaneously as phosphoinositides are lost from excised membrane patches. Previous studies have shown that currents from channels with a higher apparent affinity for PIP₂ run down slower than those with a lower apparent affinity (32). Although we could not record

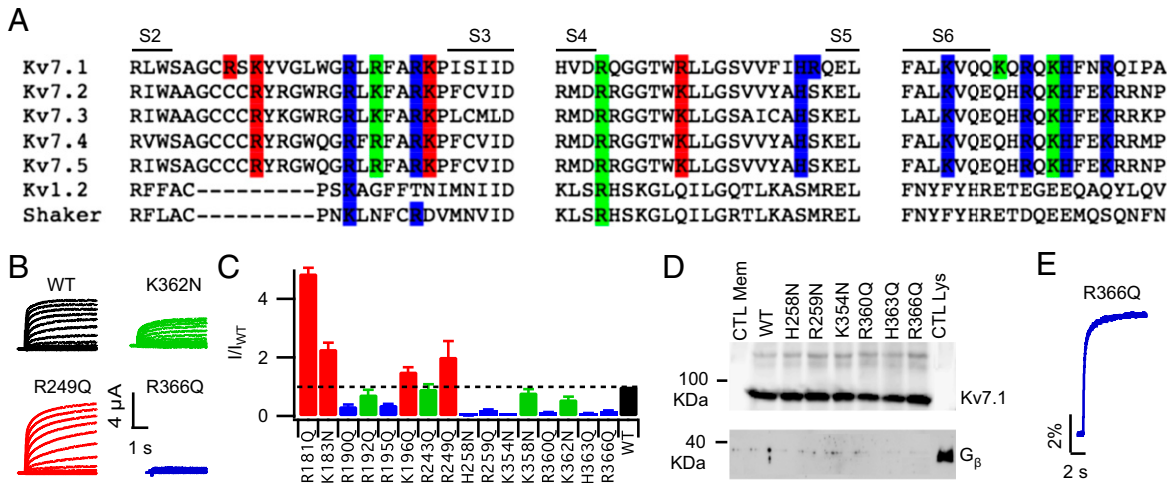


Fig. 4. Mutations at the VSD–PD interface alter channel function. (A) Sequence alignment of Kv channels S2–S3, S4–S5 linkers, and proximal C terminus. Highlighted residues were individually neutralized in WT Kv7.1. (B) Raw current at -100 to $+40$ mV. (C) Current amplitude (at $+20$ mV) normalized to WT (I/I_{WT}). Color code: blue, $I/I_{WT} < 0.5$; green, $0.5 < I/I_{WT} < 1$; red, $I/I_{WT} > 1$. (D) Western blot of biotinylated membrane proteins. CTL Mem, CTL Lys: membrane fraction and whole-cell lysate from uninjected cells. (E) $\Delta F/F$ (-80 to $+60$ mV).

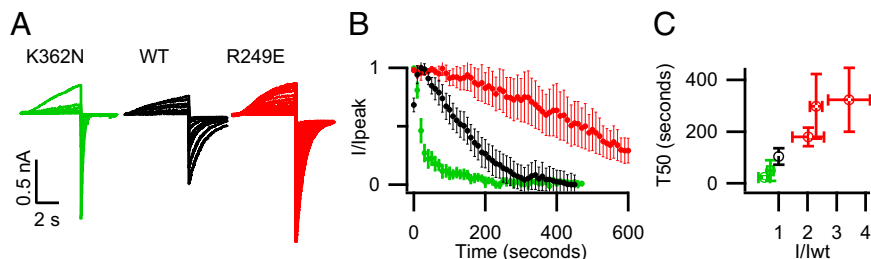


Fig. 5. Mutations at the VSD–PD interface alter apparent PIP_2 affinity. (A) Raw currents in response to repeated +80-mV pulses following excision of inside-out membrane patches. (B) Mean normalized tail current amplitude versus time following patch excision for K362N (green), WT (black), and R249E (red). (C) Time to 50% rundown versus I/I_{wt} . From Left to Right: K362N, K358N, WT, R249Q, K183N, R249E. All experiments were done in the presence of the KCNE1 subunit to slow current rundown (32) for better resolution of rundown time course.

the current rundown for the severe loss-of-current mutations, we found that the effects of other mutations (K358N, K362N, R181Q, K183N, R249Q, R249E) on the time course of rundown after patch excision were correlated with their effects on expressed current amplitude. That is, relative to WT channels, the rundown was faster for the mild loss-of-current mutations and slower for the gain-of-current mutations (Fig. 5). These results further support the hypothesis that the mutations of conserved basic residues at the VSD–PD interface affect a PIP_2 -mediated process that is required for channel function.

We directly quantified the strength of VSD–PD coupling for several of the mutations (R192Q, R195Q, K196E, K358N, K358E, R360Q, R360E, K362N, H363N, R366Q) by measuring the F – V shift caused by locking the PD open with L353K. We found that the mutations influenced VSD–PD coupling in a manner that was correlated with their effect on the expressed current amplitude; i.e., the loss-of-current mutations decreased the magnitude of the F – V shift, whereas the gain-of-current mutations increased the F – V shift (Fig. 6). Strikingly, our equilibrium model predicted

this relationship when we simply varied the binding constant for PIP_2 (K_{PIP_2}) (Fig. 6D, black line). Taken together, our results suggest that these mutations disrupt VSD–PD coupling and decrease channel current by directly affecting PIP_2 binding.

We mapped our data onto a Kv7.1 homology model (30) and found a cluster of severe loss-of-current residues at the VSD–PD interface that includes Arg190 and Arg195 in the S2–S3 linker, His258 and Arg259 in the S4–S5 linker, and Lys354 in the proximal C terminus (Fig. 7, blue). In our experiments, these mutations mimicked the effects of PIP_2 depletion on psWT channels: they severely inhibited the ionic current, did not prevent VSD activation, and greatly diminished the VSD–PD coupling. Therefore, this cluster of basic residues constitutes a critical interaction site for PIP_2 -mediated coupling. Remarkably, when we aligned the crystal structure of the voltage-independent Kir2.2 channel bound to PIP_2 (33) and the homology model of the activated-open state of Kv7.1, the PIP_2 head group from the Kir2.2 structure was centered right in the cluster (Fig. 7A and B, and Fig. S8). Furthermore, the high-impact residues His258, Arg259, and Lys354 corresponded spatially to the PIP_2 binding residues on the slide helix and the C linker of the Kir2.2 structure (Fig. S8C). These findings provide compelling evidence that our identified site is actually a PIP_2 binding site that is conserved among voltage-dependent and voltage-independent K^+ channels. The gain-of-current residues surround the PIP_2 head group when we align the Kir2.2 crystal structure with the resting-closed state model of Kv7.1 (Fig. 7C). This result suggests that neutralizing mutations at these positions increase the channel current by disrupting PIP_2 interactions that occur in the closed state. This may increase the channel current by destabilizing the closed state, or by making PIP_2 more available to bind in the pocket present in the activated-open state. The mild loss-of-current residues are located outside the conserved binding site (Fig. 7A) and likely indirectly affect PIP_2 binding at the high-impact cluster.

Discussion

Coupling is a critical process for ion channel function by which detection of a physiological stimulus within a sensor domain is transmitted to the PD to modulate channel opening. Our study identifies PIP_2 as a required factor for coupling between the VSD and PD in Kv7.1, thus expanding the current model of VSD–PD coupling to include lipid molecules. We find that PIP_2 is required for the communication of conformational energy from the VSD to the PD and from the PD to the VSD. Consistent with this finding, we identify a PIP_2 binding site at the interface between the VSD and the PD. We expect that PIP_2 binding resolves the electrostatic repulsion between the two domains, caused by the basic residues within the site, and holds the VSD in close proximity to the PD to potentiate the coupling between the two domains. The details of how PIP_2 binding potentiates coupling and precisely how VSD activation is transmitted to the pore will require further studies.

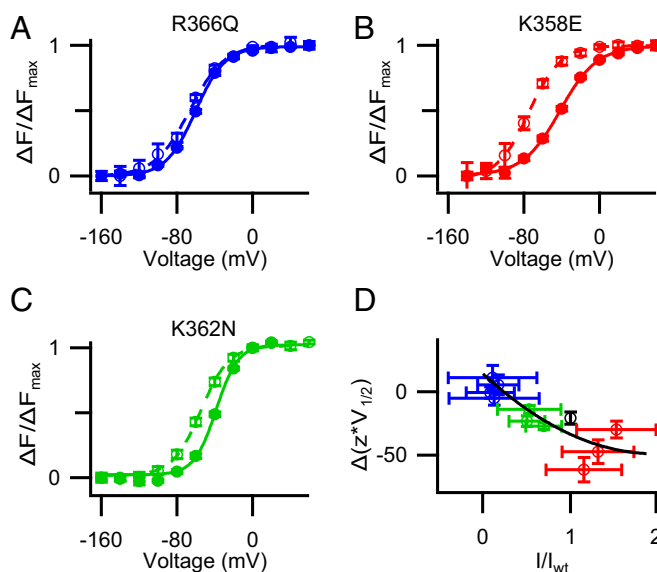


Fig. 6. Mutations at the VSD–PD interface alter coupling. Colors as in Fig. 4C. (A–C) F – V relationships of psWT/mutation (solid, filled) and psWT/L353K/mutation (dotted, open). (D) The change in $z^*V_{1/2}$ between psWT/mutation and psWT/L353K/mutation versus I/I_{wt} . From Left to Right: H363N, R195Q, R360Q, R366Q, K362N, R192Q, K358N, WT, K358E, R360E, K196N. $z^*V_{1/2}$ is a measure of the energy required to activate the VSD, where z and $V_{1/2}$ were obtained by fitting the Boltzmann equation (see Materials and Methods). The black line represents simulated data generated by varying the PIP_2 equilibrium constant (K_{PIP_2}) in the model shown in Fig. 3A.

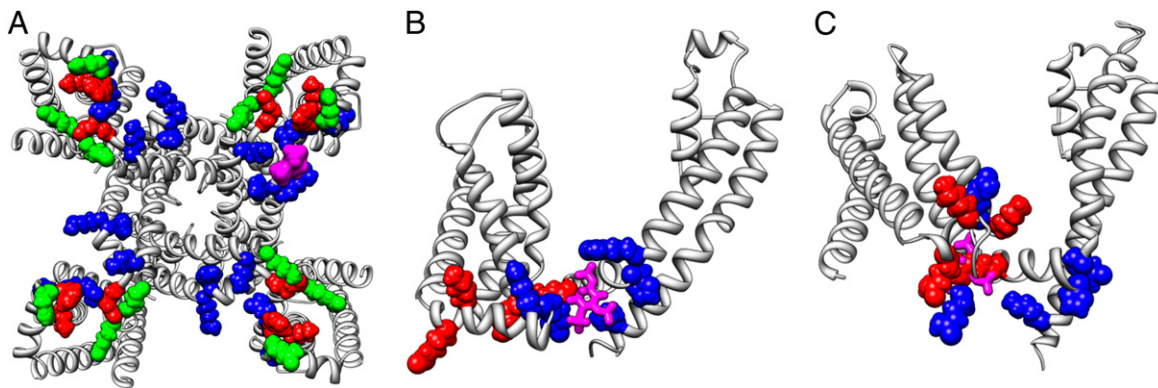


Fig. 7. Structural alignment identifies a conserved PIP₂ binding site. (A–C) Homology models of the Kv7.1 activated–open (A and B) and resting–closed (C) states (30) were aligned with the Kir2.2-PIP₂ crystal structure (33) (Fig. S8) to position the PIP₂ head group (magenta) within the models. (A) Bottom view of the activated–open model with data from Fig. 4C mapped. (B and C) Side view of one subunit from the activated–open model (B) or resting–closed model (C) with putative PIP₂ head group binding residues (blue: Arg190, Arg195, His258, Arg259, Lys354) and gain-of-current residues (red: Arg181, Lys183, Lys196, Arg249) shown.

Various ion channels, equipped with different sensor domains, require PIP₂ to open in response to stimulation. Previous studies have posited that PIP₂ stabilizes the open state of the PD, a conclusion that makes sense considering that the PD is the common element among voltage-dependent and voltage-independent K⁺ channels that required PIP₂. However, another common feature is that coupling between the conserved pore and modular sensor domains is necessary for channel function. In this study, we found that PIP₂ is required for VSD–PD coupling in the voltage-dependent Kv7.1 channel. Structural studies have suggested that PIP₂ couples the conformation of the cytosolic domain to that of the PD in voltage-independent Kir channels (33, 34). Furthermore, PIP₂ has been shown to potentiate the functional coupling in CiVSP between the VSD activation and the enzymatic activity of the cytosolic phosphatase domain (35). Therefore, we propose a general model for PIP₂ regulation of ion channels, and of some nonchannel proteins, whereby PIP₂ binding at the interface between the modular sensor and effector domains mediates functional coupling. It should be noted that not all Kv channels are PIP₂ dependent (31). Interestingly, the crystal structure of the voltage-dependent Kv1.2–2.1 chimera channel, solved in the presence of phospholipids, reveals an anionic phospholipid bound at the VSD–PD interface (36) in a position very close to our identified Kv7.1 PIP₂ interaction site (Fig. S8D). This suggests that other anionic lipids mediate VSD–PD coupling in Kv channels that do not require PIP₂.

We were able to fit our experimental data with a simple model consisting of one VSD, one PD, and one PIP₂ binding site. Initially, this was a surprising result considering that the channel is tetrameric and contains four VSDs, one PD, and, presumably, four PIP₂ sites as seen in the Kir-PIP₂ structures (33, 34). However, our data demonstrate that PIP₂ is required to link the activation of the VSD to the PD; therefore, if fewer than four PIP₂ binding sites are occupied, the PD will not be functionally coupled to all four VSDs. Indeed, the activation of Kv7.1 is far from saturated by the endogenous level of PIP₂ available in the oocyte membrane (32) such that most of the channel population may have only one PIP₂ bound and one VSD coupled. In addition, a recent study suggested that the voltage-dependent activation of Kv7.1 can be explained by an allosteric model where activation of only one VSD can open the channel (27). Thus, although our simple model is structurally inaccurate, it is a reasonable model of the channel gating at our experimental conditions and recapitulates the important features of the data.

PIP₂-mediated coupling in Kv7.1 has direct implications for human pathophysiology. In the heart, Kv7.1 subunits coassemble

with KCNE1 accessory subunits to generate the slow delayed rectifier current (I_{Ks}) (37, 38) that regulates the duration of the cardiac action potential. Inherited loss-of-function mutations of Kv7.1 and KCNE1 are associated with long QT syndrome (LQT), in which the ventricular action potential duration is prolonged, resulting in a high risk of ventricular arrhythmias and sudden death. Eleven previously reported LQT-associated mutations (39–46) affect basic residues in the PIP₂ pocket (Table S1). For these mutations, loss of VSD–PD coupling may compromise the I_{Ks} channel function and create a substrate for cardiac arrhythmias. Our results demonstrate that modifiers of VSD activation will not rescue channel function for these mutations. Furthermore, drugs that force the PD open will abolish the voltage and time dependence of the I_{Ks} current that is critical for the timing of the action potential (47). However, if a drug could target the PIP₂-dependent coupling, it would amplify the current without losing these physiologically important characteristics. This is an exciting rationale for drug design that may be applicable to other PIP₂-related ion channel diseases (48).

Materials and Methods

Mutagenesis. Site-directed mutations were introduced using overlap extension and high-fidelity PCR. DNA sequencing confirmed each mutation. RNA was made by *in vitro* transcription using the mMessage mMachine T7 polymerase kit (Applied Biosystems).

Channel Expression. A total of 9.2 ng of channel cRNA was injected, using Nanoject (Drummond), into each of stage V–VI, defolliculated oocytes from *Xenopus laevis*. For expression of CiVSP, 2.3 ng of CiVSP RNA was injected simultaneously. The cells were incubated at 18 °C for 4–7 d for robust expression in ND96 solution (in mM: 96 NaCl, 2 KCl, 1.8 CaCl₂, 1 MgCl₂, 5 Hepes, 0.3 K₂EDTA).

Electrophysiology Two-electrode voltage clamp. Whole-cell currents were recorded from oocytes bathed in ND96 solution using a CA-B amplifier (Dagan) in two-electrode voltage-clamp mode. Microelectrodes were pulled to a resistance of 0.3–3 MΩ and filled with 3 mM KCl. Signals were sampled at 1 kHz using the Patchmaster acquisition software (HEKA). The holding potential was set to –80 mV throughout, unless otherwise specified.

Voltage-clamp fluorometry. For voltage-clamp fluorometry, oocytes were labeled on ice for 45 min in 10 μM Alexa 488 C5 maleimide (Life Technologies) in high-potassium depolarizing solution (in mM: 98 KCl, 1.8 CaCl₂, 1 MgCl₂, 5 Hepes, pH 7.6). The cells were washed with ND96 and kept on ice until recording. Fluorescent signals were recorded simultaneously with the whole-cell (TEVC) currents in ND96 solution, using a DLMFS (Leica) upright microscope through a FITC filter cube (Leica). Light from a standard 100-W halogen bulb was focused onto the animal pole of the oocyte and emission from the cube was focused on a P20A photodiode. The current from the

photodiode was amplified using an EPC10 patch amplifier (HEKA), low-pass filtered at 200 Hz, and sampled at 1 kHz using Patchmaster (HEKA).

Patch clamp. Inside-out membrane patches were formed using patch electrodes pulled to 0.5–1 MΩ and filled with pipette solution (in mM: 140 KMeSO₃, 20 Hepes, 2 KCl, 2 MgCl₂, pH 7.2) and excised into the bathing solution (in mM: 140 KMeSO₃, 20 Hepes, 2 KCl, 5 EGTA, 1.5 mM MgATP, pH 7.2). Macroscopic currents were recorded, at room temperature, using an Axopatch 200-B amplifier (Axon Instruments) driven by the Pulse (HEKA) acquisition software. Currents were digitized at 1 kHz.

All recordings were made in room temperature (20–22 °C).

Data Analysis. The baseline fluorescence was fit with a line during the 2 s at the –80-mV holding potential that preceded each test pulse. This linear baseline approximation was extrapolated to the duration of the pulse and ΔF/F was calculated as $(F(t) - F_{\text{baseline}}(t))/F_{\text{baseline}}(t)$, where $F(t)$ is the fluorescent intensity at time t (in arbitrary units) and $F_{\text{baseline}}(t)$ is the extrapolated baseline value at time t .

The Boltzmann equation was used to fit the fluorescence–voltage relationships: Normalized $\Delta F(V) = PV_a(V) = 1/(1 + \exp(-z^*F^*(V - V_{1/2})/RT))$, where PV_a is the voltage-dependent probability of the voltage sensor assuming the activated state, V is the test voltage (in volts), $V_{1/2}$ is the voltage of half-maximal voltage sensor activation, z is the number of elementary charges translocated across the membrane upon VSD activation, R is the gas constant (in joules per kelvin per mole), and F is the faraday constant (in coulombs per mole).

- Long SB, Campbell EB, Mackinnon R (2005) Crystal structure of a mammalian voltage-dependent Shaker family K⁺ channel. *Science* 309(5736):897–903.
- Payandeh J, Scheuer T, Zheng N, Catterall WA (2011) The crystal structure of a voltage-gated sodium channel. *Nature* 475(7356):353–358.
- Larsson HP, Baker OS, Dhillon DS, Isacoff EY (1996) Transmembrane movement of the shaker K⁺ channel S4. *Neuron* 16(2):387–397.
- Liu Y, Holmgren M, Jurman ME, Yellen G (1997) Gated access to the pore of a voltage-dependent K⁺ channel. *Neuron* 19(1):175–184.
- Jiang Y, et al. (2002) The open pore conformation of potassium channels. *Nature* 417(6888):523–526.
- Shaya D, et al. (2011) Voltage-gated sodium channel (Na_v) protein dissection creates a set of functional pore-only proteins. *Proc Natl Acad Sci USA* 108(30):12313–12318.
- Sasaki M, Takagi M, Okamura Y (2006) A voltage sensor-domain protein is a voltage-gated proton channel. *Science* 312(5773):589–592.
- Ramsey IS, Moran MM, Chong JA, Clapham DE (2006) A voltage-gated proton-selective channel lacking the pore domain. *Nature* 440(7088):1213–1216.
- Ledwell JL, Aldrich RW (1999) Mutations in the S4 region isolate the final voltage-dependent cooperative step in potassium channel activation. *J Gen Physiol* 113(3):389–414.
- Lu Z, Klem AM, Ramu Y (2001) Ion conduction pore is conserved among potassium channels. *Nature* 413(6858):809–813.
- Long SB, Campbell EB, Mackinnon R (2005) Voltage sensor of Kv1.2: Structural basis of electromechanical coupling. *Science* 309(5736):903–908.
- Soler-Llavina GJ, Chang T-H, Swartz KJ (2006) Functional interactions at the interface between voltage-sensing and pore domains in the Shaker Kv channel. *Neuron* 52(4):623–634.
- Grabe M, Lai HC, Jain M, Nung Jan Y, Yeh Jan L (2007) Structure prediction for the down state of a potassium channel voltage sensor. *Nature* 445(7127):550–553.
- Suh B-C, Hille B (2008) PIP₂ is a necessary cofactor for ion channel function: How and why? *Annu Rev Biophys* 37:175–195.
- Wang Q, et al. (1996) Positional cloning of a novel potassium channel gene: *KVLQT1* mutations cause cardiac arrhythmias. *Nat Genet* 12(1):17–23.
- Delmas P, Brown DA (2005) Pathways modulating neural KCNQ/M (Kv7) potassium channels. *Nat Rev Neurosci* 6(11):850–862.
- Zhang H, et al. (2003) PIP₂ activates KCNQ channels, and its hydrolysis underlies receptor-mediated inhibition of M currents. *Neuron* 37(6):963–975.
- Mannuzzu LM, Moronne MM, Isacoff EY (1996) Direct physical measure of conformational rearrangement underlying potassium channel gating. *Science* 271(5246):213–216.
- Osteen JD, et al. (2010) KCNE1 alters the voltage sensor movements necessary to open the KCNQ1 channel gate. *Proc Natl Acad Sci USA* 107(52):22710–22715.
- Murata Y, Iwasaki H, Sasaki M, Inaba K, Okamura Y (2005) Phosphoinositide phosphatase activity coupled to an intrinsic voltage sensor. *Nature* 435(7046):1239–1243.
- Iwasaki H, et al. (2008) A voltage-sensing phosphatase, Ci-VSP, which shares sequence identity with PTEN, dephosphorylates phosphatidylinositol 4,5-bisphosphate. *Proc Natl Acad Sci USA* 105(23):7970–7975.
- Rocheleau JM, Kobertz WR (2008) KCNE peptides differently affect voltage sensor equilibrium and equilibration rates in KCNQ1 K⁺ channels. *J Gen Physiol* 131(1):59–68.
- Arcisio-Miranda M, Muroi Y, Chowdhury S, Chanda B (2010) Molecular mechanism of allosteric modification of voltage-dependent sodium channels by local anesthetics. *J Gen Physiol* 136(5):541–554.
- Ryu S, Yellen G (2012) Charge movement in gating-locked HCN channels reveals weak coupling of voltage sensors and gate. *J Gen Physiol* 140(5):469–479.
- Boulet IR, Labro AJ, Raes AL, Snyders DJ (2007) Role of the S6 C-terminus in KCNQ1 channel gating. *J Physiol* 585(Pt 2):325–337.
- Lecher C, et al. (2007) Chromanol 293B binding in KCNQ1 (Kv7.1) channels involves electrostatic interactions with a potassium ion in the selectivity filter. *Mol Pharmacol* 71(6):1503–1511.
- Osteen JD, et al. (2012) Allosteric gating mechanism underlies the flexible gating of KCNQ1 potassium channels. *Proc Natl Acad Sci USA* 109(18):7103–7108.
- Ruscic KJ, et al. (2013) I_{Ks} channels open slowly because KCNE1 accessory subunits slow the movement of S4 voltage sensors in KCNQ1 pore-forming subunits. *Proc Natl Acad Sci USA* 110(7):E559–E566.
- Rosenhouse-Dantsker A, Logothetis DE (2007) Molecular characteristics of phosphoinositide binding. *Pflügers Arch* 455(1):45–53.
- Smith J, Vanoye CG, George AL Jr., Meiler AL, Sanders CR (2007) Structural models for the KCNQ1 voltage-gated potassium channel. *Biochemistry* 46(49):14141–14152.
- Kruse M, Hammond GRV, Hille B (2012) Regulation of voltage-gated potassium channels by PI(4,5)P₂. *J Gen Physiol* 140(2):189–205.
- Li Y, et al. (2011) KCNE1 enhances phosphatidylinositol 4,5-bisphosphate (PIP₂) sensitivity of I_{Ks} to modulate channel activity. *Proc Natl Acad Sci USA* 108(22):9095–9100.
- Hansen SB, Tao X, Mackinnon R (2011) Structural basis of PIP₂ activation of the classical inward rectifier K⁺ channel Kir2.2. *Nature* 477(7365):495–498.
- Whorton MR, Mackinnon R (2011) Crystal structure of the mammalian GIRK2 K⁺ channel and gating regulation by G proteins, PIP₂, and sodium. *Cell* 147(1):199–208.
- Kohout SC, et al. (2010) Electrochemical coupling in the voltage-dependent phosphatase Ci-VSP. *Nat Chem Biol* 6(5):369–375.
- Long SB, Tao X, Campbell EB, Mackinnon R (2007) Atomic structure of a voltage-dependent K⁺ channel in a lipid membrane-like environment. *Nature* 450(7168):376–382.
- Sanguinetti MC, et al. (1996) Coassembly of KvLQT1 and minK (I_sK) proteins to form cardiac I_{Ks} potassium channel. *Nature* 384(6604):80–83.
- Barhanin J, et al. (1996) KvLQT1 and I_sK (minK) proteins associate to form the I_{Ks} cardiac potassium current. *Nature* 384(6604):78–80.
- Chouabe C, et al. (2000) Novel mutations in KvLQT1 that affect I_{Ks} activation through interactions with I_sK. *Cardiovasc Res* 45(4):971–980.
- Napolitano C, et al. (2005) Genetic testing in the long QT syndrome: Development and validation of an efficient approach to genotyping in clinical practice. *JAMA* 294(23):2975–2980.
- Millat G, et al. (2006) Spectrum of pathogenic mutations and associated polymorphisms in a cohort of 44 unrelated patients with long QT syndrome. *Clin Genet* 70(3):214–227.
- Kubota T, Shimizu W, Kamakura S, Horie M (2000) Hypokalemia-induced long QT syndrome with an underlying novel missense mutation in S4–S5 linker of KCNQ1. *J Cardiovasc Electrophysiol* 11(9):1048–1054.
- Choi G, et al. (2004) Spectrum and frequency of cardiac channel defects in swimming-triggered arrhythmia syndromes. *Circulation* 110(15):2119–2124.
- Splawski I, et al. (2000) Spectrum of mutations in long-QT syndrome genes. *KVLQT1*, *HERG*, *SCN5A*, *KCNE1*, and *KCNE2*. *Circulation* 102(10):1178–1185.
- Splawski I, et al. (1998) Genomic structure of three long QT syndrome genes: *KVLQT1*, *HERG*, and *KCNE1*. *Genomics* 51(1):86–97.
- Tanaka T, et al. (1997) Four novel *KVLQT1* and four novel *HERG* mutations in familial long-QT syndrome. *Circulation* 95(3):565–567.
- Silva J, Rudy Y (2005) Subunit interaction determines I_{Ks} participation in cardiac repolarization and repolarization reserve. *Circulation* 112(10):1384–1391.
- Logothetis DE, Petrou VI, Adney SK, Mahajan R (2010) Channelopathies linked to plasma membrane phosphoinositides. *Pflügers Arch* 460(2):321–341.
- Wu D, et al. (2010) State-dependent electrostatic interactions of S4 arginines with E1 in S2 during Kv7.1 activation. *J Gen Physiol* 135(6):595–606.

Statistical comparison was done using a Student *t* test. Errors represent SEM throughout.

Chemical Modification. MTSES (Toronto Research Chemicals) was dissolved in DMSO at 100 mM, aliquoted, and frozen immediately. Aliquots were thawed just before use and added directly to bath solution in a bolus to achieve the desired final concentration.

Biotinylation and Western Blot. Membrane expression was detected through biotinylation and Western blot (49). Cell surface proteins of intact oocytes were labeled with 1 mg/mL sulfo-NHS-SS-biotin (Thermo Scientific). The cells were washed, homogenized, and incubated with NeutrAvidin beads (Thermo Scientific) to pull down biotin-labeled proteins. The pulled-down proteins were probed via Western blot using a Kv7.1 antibody (Santa Cruz Biotechnology) or a Gβ antibody to test for labeling of cytosolic proteins.

ACKNOWLEDGMENTS. We thank Dr. Y. Okamura (Osaka University) for the CivSP clone and Dr. S. Goldstein (Brandeis University) for the KCNQ1 clone. We also thank Drs. J. Nerbonne and A. Federman for review of the manuscript, and A. Krumholz for many excellent discussions throughout this project. This study was funded by an Established Investigator Award 0440066N from the American Heart Association, Grants R01-HL70393 and R01-NS060706 from National Institutes of Health (to J.C.), Burroughs Wellcome Fund 1010299 (to J.R.S.), and American Heart Association Predoctoral Fellowship 11PRE5720009 (to M.A.Z.). J.C. is the Professor of Biomedical Engineering on the Spencer T. Olin Endowment.

Supporting Information

Zayzman et al. 10.1073/pnas.1305167110

SI Materials and Methods

Derivation and Fitting of Model Parameters. The model in Fig. S6 consists of eight states and four parameters (K_v , K_g , K_p , θ); K_v is voltage dependent:

$$K_v = K_{v0} * \exp(zFV/RT),$$

where K_{v0} is the equilibrium constant for voltage-sensing domain (VSD) activation in the absence of applied voltage, z is the amount of gating charge associated with the activation of the VSD, F is the faraday constant, V is the voltage, R is the universal gas constant, and T is the absolute temperature.

Assuming two states (resting and activated) for the voltage sensor, the two parameters (K_{v0} and z) can be measured directly by fitting the experimental fluorescence data for VSD activation after depletion of endogenous phosphatidylinositol 4,5-bisphosphate (PIP₂) by the voltage sensing phosphatase from *Ciona intestinalis* (CiVSP) as follows:

$$\begin{aligned} K_v &= \frac{P(V_a)}{P(V_r)} = \frac{P(V_a)}{1 - P(V_a)} = \frac{\Delta F}{1 - \Delta F} \\ \Delta F &= \frac{K_v}{1 + K_v} = \frac{K_{v0} * e^{zFV/RT}}{1 + K_{v0} * e^{zFV/RT}}. \end{aligned}$$

The best fit to the pseudo-wild-type (psWT) + CiVSP F - V data were achieved when $K_{v0} = 45.12$ and $z = 1.866$ (not shown). To find the remaining three free parameters (K_g , K_p , θ), the parameter space was searched by fitting three sets of data as described below: the G - V of the psWT channels, the F - V s of psL353K and psWT channels under conditions of endogenous and depleted PIP₂, and the activity response relationship of WT channels to exogenous PIP₂.

In our experiments, we do not measure open probability (PPo) directly. Instead, the G - V relationship (Fig. 3C, Upper) represents the conductance at each voltage relative to the conductance at saturating voltages (PPo/PPo_{max}). Equations can be derived for the probability of pore domain (PD) opening (PPo) at all voltage and at saturating voltages providing a means to fit the experimentally measured G - V relationship as follows:

$$\frac{PPo}{PPo_{max}} = \frac{\frac{K_g + K_v * K_g + K_p * K_g + \theta * K_v * K_p * K_g}{1 + K_v + K_g + K_p + K_v * K_g + K_v * K_p + K_g * K_p + \theta * K_v * K_p * K_g}}{\frac{K_g + \theta * K_p * K_g}{1 + K_g + K_p + \theta * K_p * K_g}}.$$

The F - V relationships (Fig. 3C, Lower) are fit to an equation for the probability of VSD activation (PVa). Assuming that voltage can drive the conformation of the VSD fully toward the resting or activated state, the experimentally measured F - V relationship reports directly on PVa as follows:

$$PVa = \frac{K_v + K_v * K_g + K_v * K_p + \theta * K_v * K_p * K_g}{1 + K_v + K_g + K_p + K_v * K_g + K_v * K_p + K_g * K_p + \theta * K_v * K_p * K_g}.$$

The PIP₂ activity response data (Fig. 3B) was measured experimentally by applying various concentrations of exogenous PIP₂ to the intracellular face of excised membrane patches and measuring the steady-state current elicited by the voltage pulse from -80 to $+80$ mV (1), fitting the dose-response curve requires an equation for the difference current between low (-80 mV) and high ($+80$ mV) voltages (PPo_{diff}) as follows:

$$\begin{aligned} PPo_{diff} &= \frac{PPo}{V \rightarrow \infty} - \frac{PPo}{V \rightarrow -\infty} \\ &= \frac{K_g + \theta * K_p * K_g}{1 + K_g + K_p + \theta * K_p * K_g} - \frac{K_g + K_p * K_g}{1 + K_g + K_p + K_p * K_g}. \end{aligned}$$

Experimentally, the response at each level of PIP₂ is normalized to the maximal response at saturating PIP₂ concentrations (estimated by fitting the Hill equation to the data due to the saturating concentration being beyond the limit of solubility for PIP₂). Therefore, the normalized dose-response data (Fig. 3B) are fit with the following equation:

$$\frac{PPo_{diff}}{PPo_{diff} \atop K_p \rightarrow \infty} = \frac{\frac{K_g + \theta * K_p * K_g}{1 + K_g + K_p + \theta * K_p * K_g} - \frac{K_g + K_p * K_g}{1 + K_g + K_p + K_p * K_g}}{\frac{\theta * K_g}{1 + \theta * K_g} - \frac{K_g}{1 + K_g}}.$$

To fit the data with this equation, it is necessary to relate the concentration of exogenous PIP₂ to an equivalent value of K_p . To do so, we assume a linear function for the partitioning of PIP₂ from the bath solution into the patch membrane and that K_p depends linearly on the membrane concentration of PIP₂ in the membrane. Therefore, K_p can be related to PIP₂ concentrations in solution by a simple aggregate linear coefficient D as follows:

$$[MembranePIP2] = K_1 * [SolutionPIP2]$$

$$\begin{aligned} K_p &= K_{p0} * [MembranePIP2] = K_{p0} * K_1 * [SolutionPIP2] \\ &= D * [SolutionPIP2]. \end{aligned}$$

The value for D can be estimated by using the experimentally measured concentration of PIP₂ in solution that yields the half-maximal activity (EC₅₀ of 596 μ M, estimated by fitting the Hill equation with nH = 1). An implicit equation for the equivalent K_p providing half-maximal activity can be derived and solved for as a function of K_g and θ (for $K_g = 0.02$ and $\theta = 8$, $D = 689 \mu M^{-1}$).

A single set of parameters was identified that provided satisfying fits to the experimental data (Fig. 3B). The effects of L353K

on the channel were simulated by increasing K_g (from 0.02 to 1,000), whereas the effects of CiVSP were simulated by de-

creasing K_{PIP_2} (from 0.75 to 0.01). All other parameters were kept constant (values listed in Fig. S6).

- Li Y, et al. (2011) KCNE1 enhances phosphatidylinositol 4,5-bisphosphate (PIP2) sensitivity of IKs to modulate channel activity. *Proc Natl Acad Sci USA* 108(22):9095–9100.

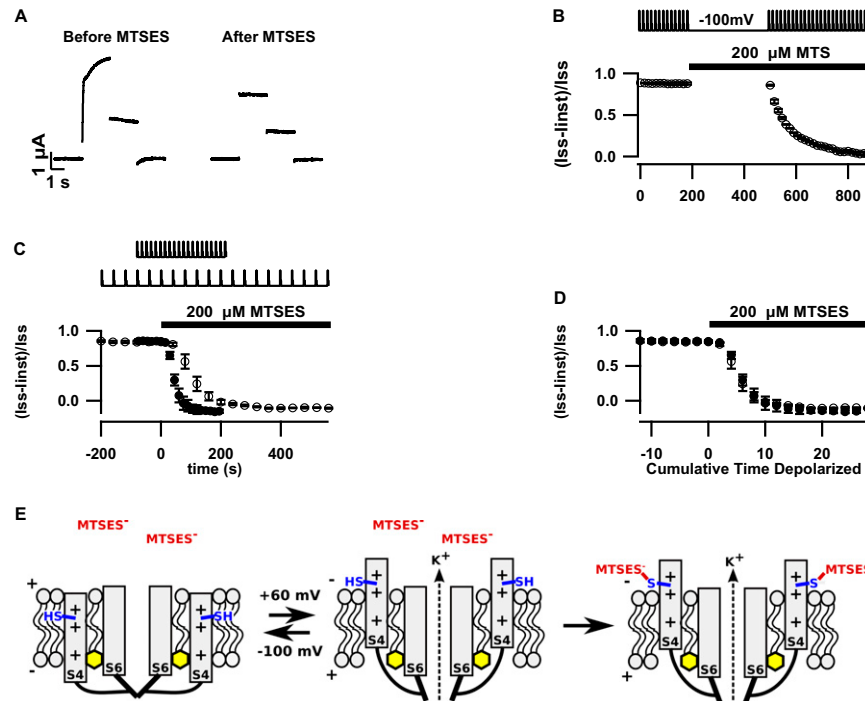


Fig. S1. VSD activation detected by accessibility of 2-sulfanatoethyl methanethiosulfonate (MTSES) to I230C in S4. (A) Exposure of mutant, C214A/I230C/C331A, channels to 200 μ M MTSES rapidly converts the channel current from time dependent to time independent after repeated pulses to +60 mV for 2 s every 15 s, from a holding potential of -100 mV. In contrast, exposure of C214A/C331A channels to 200 μ M MTSES does not modify channel current. (B) Holding the membrane potential at -100 mV during exposure of C136/I230C/C331A channels to MTSES prevents the modification of I230C, indicating that C230 is accessible to MTSES only at the activated state. I_{ss}, steady-state current at the end of the +60-mV pulse; I_{inst}, instantaneous current at the beginning of the +60-mV pulse. (C) Time-dependent current fraction [$(I_{ss} - I_{inst})/I_{ss}$] plotted versus time for an interpulse interval of 15 s (filled symbols) and 40 s (open symbols) showing that increasing the time in between the +60-mV pulses from 15 to 40 s slows the rate of modification (filled to open symbols). (D) Data in C replotted versus cumulative time at depolarized potentials demonstrating that that the modification depends on the total time spent at the depolarized voltage and not the time in between the depolarizing pulses. (E) Cartoons illustrating the interpretation of the experimental results: MTSES (red), I230C (blue), PIP₂ (yellow).

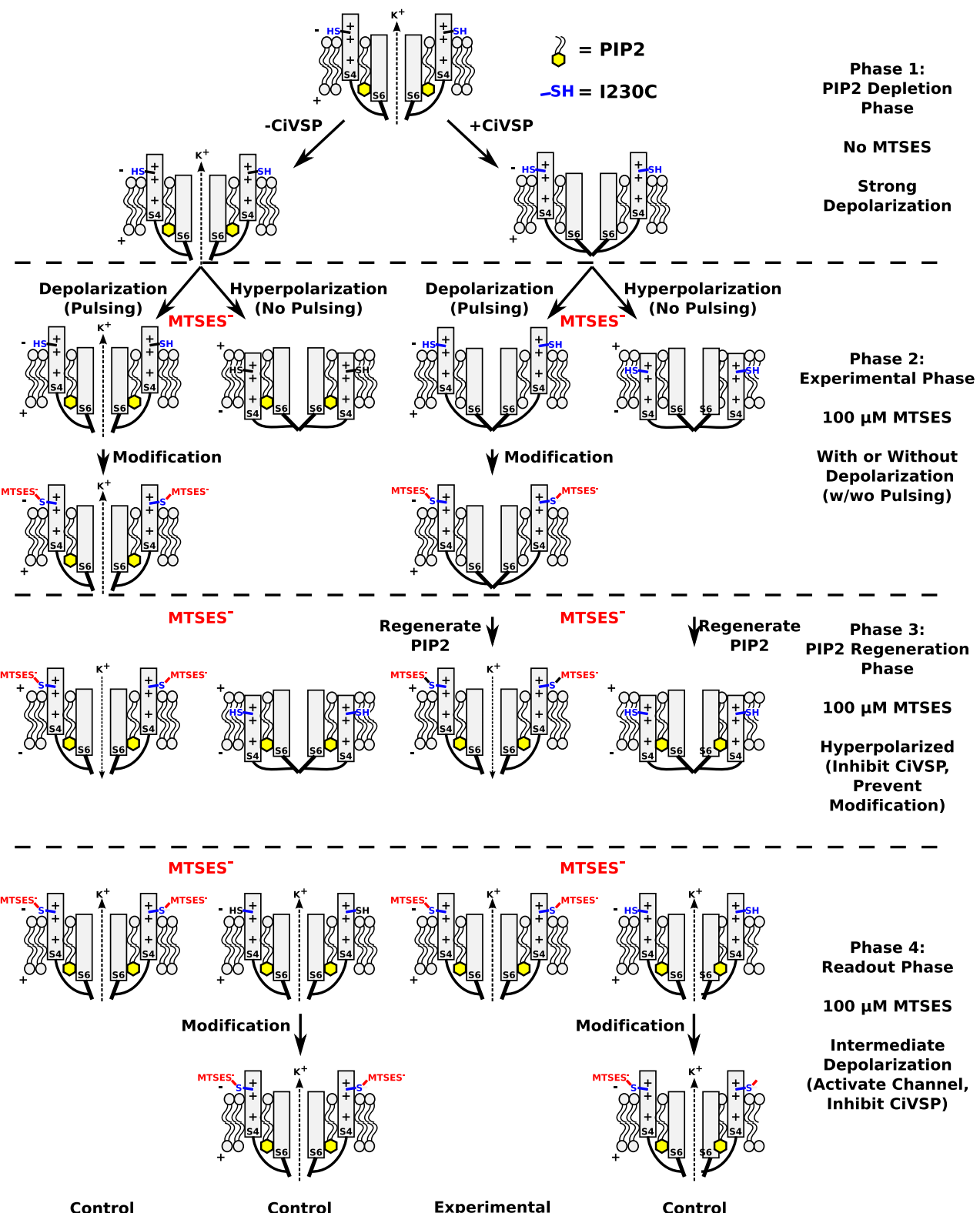


Fig. S2. Using chemical modification to test for VSD activation after PIP₂ depletion. In phase 1, cells expressing C214A/I230C/C331A channels alone or with CiVSP are subjected to strong (60 mV) depolarizing pulses to activate CiVSP (if present) and deplete endogenous PIP₂. In phase 2, 100 μM MTSES is applied in the bath solutions while the membrane potential is held at -100 mV or depolarized (pulsed) to 60 mV. If the VSD can be activated after PIP₂ depletion, the exposure of I230C in the S4 to the extracellular solution will result in chemical modification that would remain undetected as PIP₂ depletion eliminates the ionic current. In phase 3, the membrane potential is held at -100 mV to deactivate the VSDs and prevent further modification while also deactivating CiVSP to allow the endogenous lipid kinases to regenerate PIP₂ in the membrane. In phase 4, the membrane potential is pulsed to an intermediate potential, -20 mV, at which the channel is activated and CiVSP activity is low. Under these conditions, movement and modification of the VSD in phase 2 will be detected as less time-dependent current and less subsequent modification compared with the control where the membrane potential is held at -100 mV in phase 2.

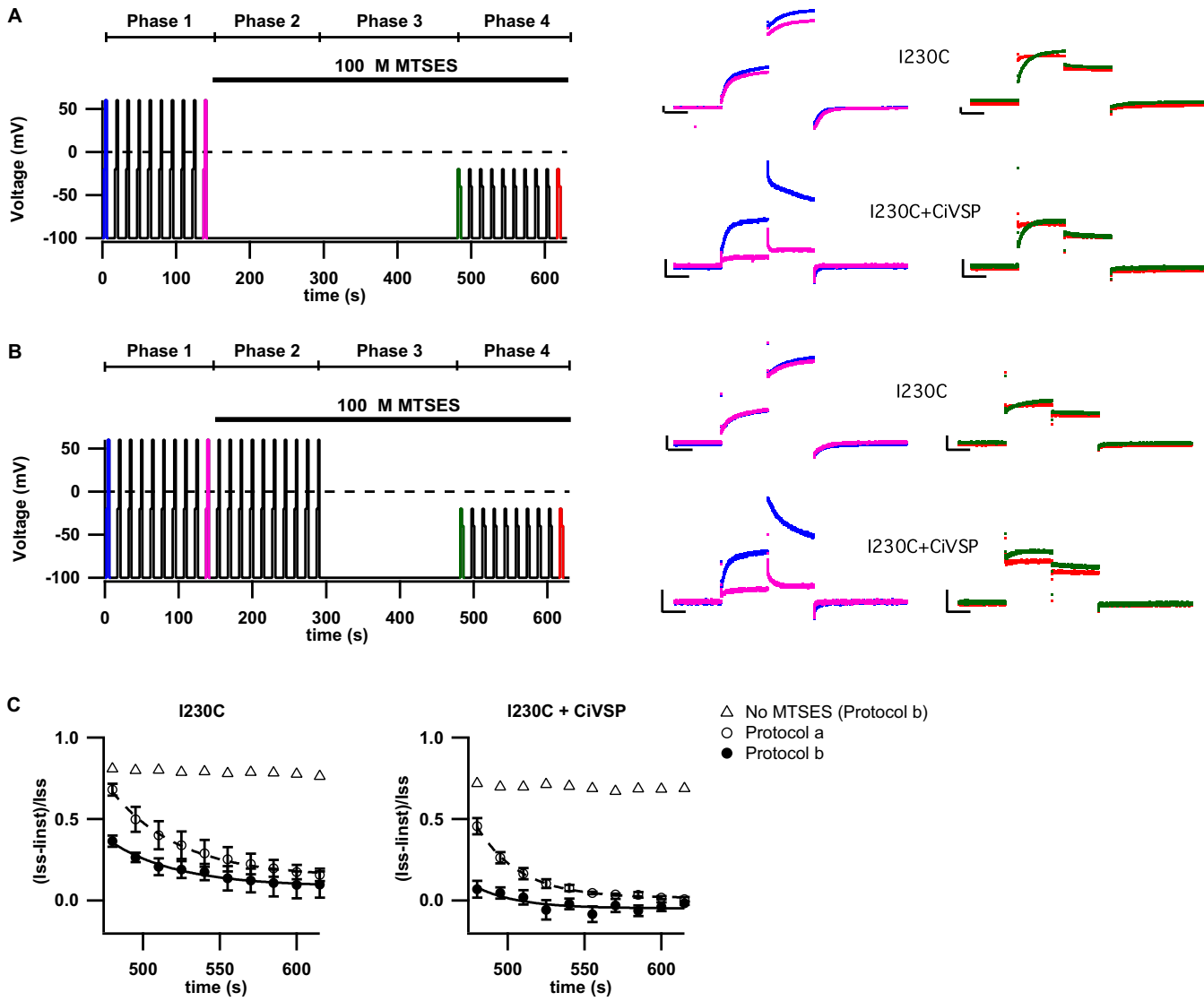


Fig. S3. VSD activation occurs after PIP_2 depletion as detected by chemical modification. Oocytes expressing C214A/I230C/C331A channels alone (I230C) or with CiVSP (I230C + CiVSP) were subjected to the four-phase experiment described in Fig. S2. (A and B) The four-phase voltage protocol (Left) and example currents at various times during the experiment (Right; the current traces were elicited by the voltage pulses highlighted in the same color). In phase 1, the PIP_2 depletion phase, we applied 10 pulses consisting of a 2-s depolarizing membrane potential to -20 mV (VSDs activated, low CiVSP activity) from the -100 mV holding potential (VSDs resting, low CiVSP activity) followed by a further depolarization to $+60\text{ mV}$ (VSDs activated, high CiVSP activity) for 2 s. These 10 pulses established a steady state of depleted PIP_2 levels in the presence of CiVSP as indicated by the reduction of the ionic currents [compare the currents at the first (blue) and the 10th (magenta) pulses]. In phase 2, the experimental phase, $100\text{ }\mu\text{M}$ MTSES was added to the extracellular solution while the membrane potential was held at -100 mV (control, VSDs resting) (A) or depolarized with an additional 10 depolarizing pulses as in phase 1 to activate VSDs (B). In phase 3, the PIP_2 regeneration phase, membrane potential was held at -100 mV (VSDs resting, low CiVSP activity) to allow the regeneration of PIP_2 by the endogenous lipid kinases. In phase 4, the readout phase, we applied 10 repeated pulses consisting of a -20-mV depolarization for 2 s (VSDs activated, low CiVSP activity) followed by a -40-mV (VSDs activated, low CiVSP activity) potential for 2 s to assay for VSD modification that had occurred in phase 2. Currents at the first pulse (green) and the 10th pulse (red) show the changes in the time-dependent component in response to the -20-mV depolarization. In A, the currents elicited by the first pulse (green) both in the presence and absence of CiVSP contain a substantial time-dependent component, indicating that a large fraction of the channels had not been modified by MTSES due to VSD being held at the resting state by the hyperpolarized membrane potential in phase 2. However, in B, the currents elicited by the first pulse (green) contain little time-dependent component both in the presence and absence of CiVSP, indicating that most of the channels had been modified by MTSES due to VSD activation in phase 2 regardless of PIP_2 depletion. (C) The averaged fraction of time-dependent current is plotted versus time for the 10 pulses in phase 4 for the protocol in A (open circles) and B (closed circles). Also plotted are the results of control experiments using the protocol in B but with no MTSES addition (no MTSES, open triangles). Iss, steady-state current at the end of the -20-mV pulse; linst, instantaneous current at the beginning of the -20-mV pulse. It is clear that in the presence of CiVSP that had depleted PIP_2 (Right) the protocol in B yielded less time-dependent current than the protocol in A, indicating that the accessibility of I230C to MTSES is voltage dependent. Therefore, depletion of endogenous PIP_2 by CiVSP did not prevent VSD activation.

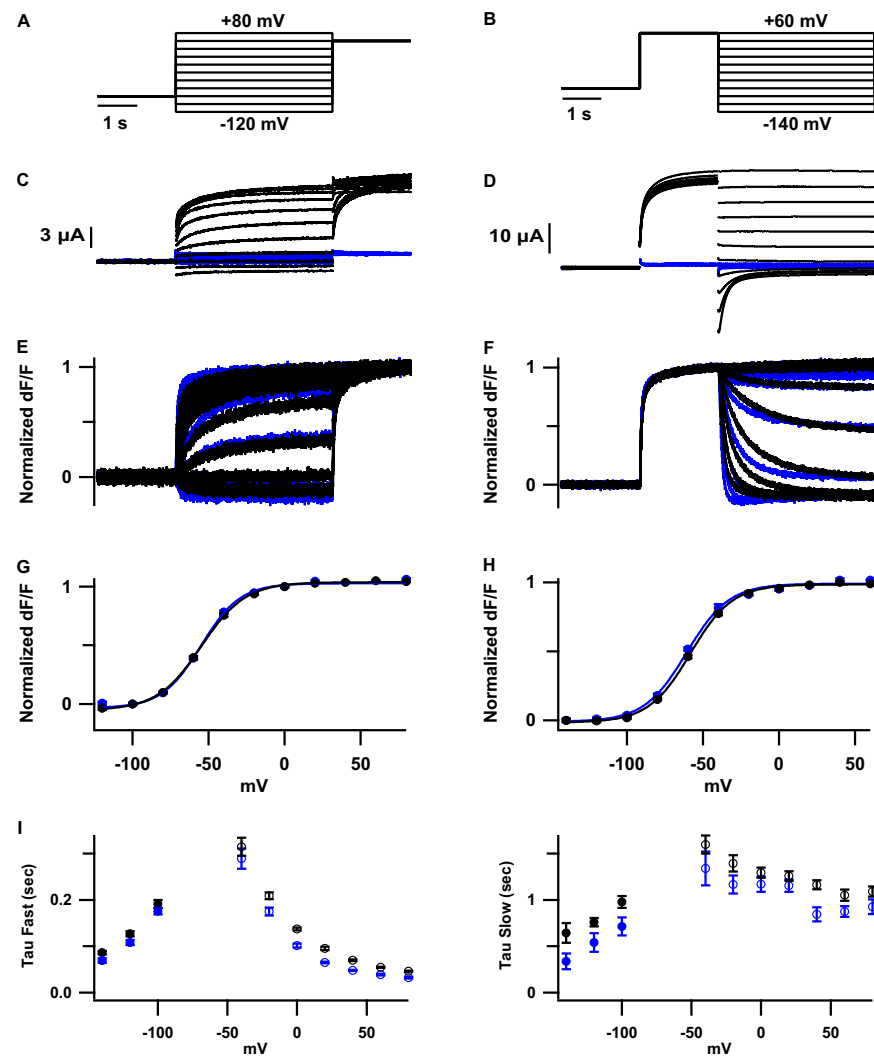


Fig. S4. Effects of PIP_2 depletion on voltage-dependent gating. Voltage-clamp fluorometry recordings of psWT (black) or psWT + CiVSP (blue). The protocols were designed to deplete PIP_2 in the presence of CiVSP by first applying six voltage pulses as in Fig. 1B. (A) Voltage protocol used in A, C, E, and G, and Fig. 3C, Lower. The membrane potential is stepped from a holding potential of -80 mV to various test potentials (-120 to $+80$ mV) for 4 s and then to $+60$ mV for 2 s to activate CiVSP. (B) Voltage protocol used in D, F, and H, and Fig. 2C. The membrane is stepped from a holding potential of -80 to $+60$ mV for 2 s to activate the VSDs and CiVSP. The membrane potential is then repolarized to various test potentials (-140 to $+60$ mV) to track the return of the VSD to the resting state. (C and D) Raw currents. (E and F) $\Delta F/F$. Signals are normalized to that at the end of the $+60$ -mV pulse (E) or prepulse (F). (G and H) Normalized F - V relationships. Signals at the end of the 4-s test pulses are normalized to that at 0 mV and plotted versus test voltage. (I) Fast (Left) and slow (Right) τ of the double exponential fit to the fluorescent signal changes caused by depolarization (-40 to $+80$ mV) or repolarization (-140 to -100 mV) are plotted versus test voltage.

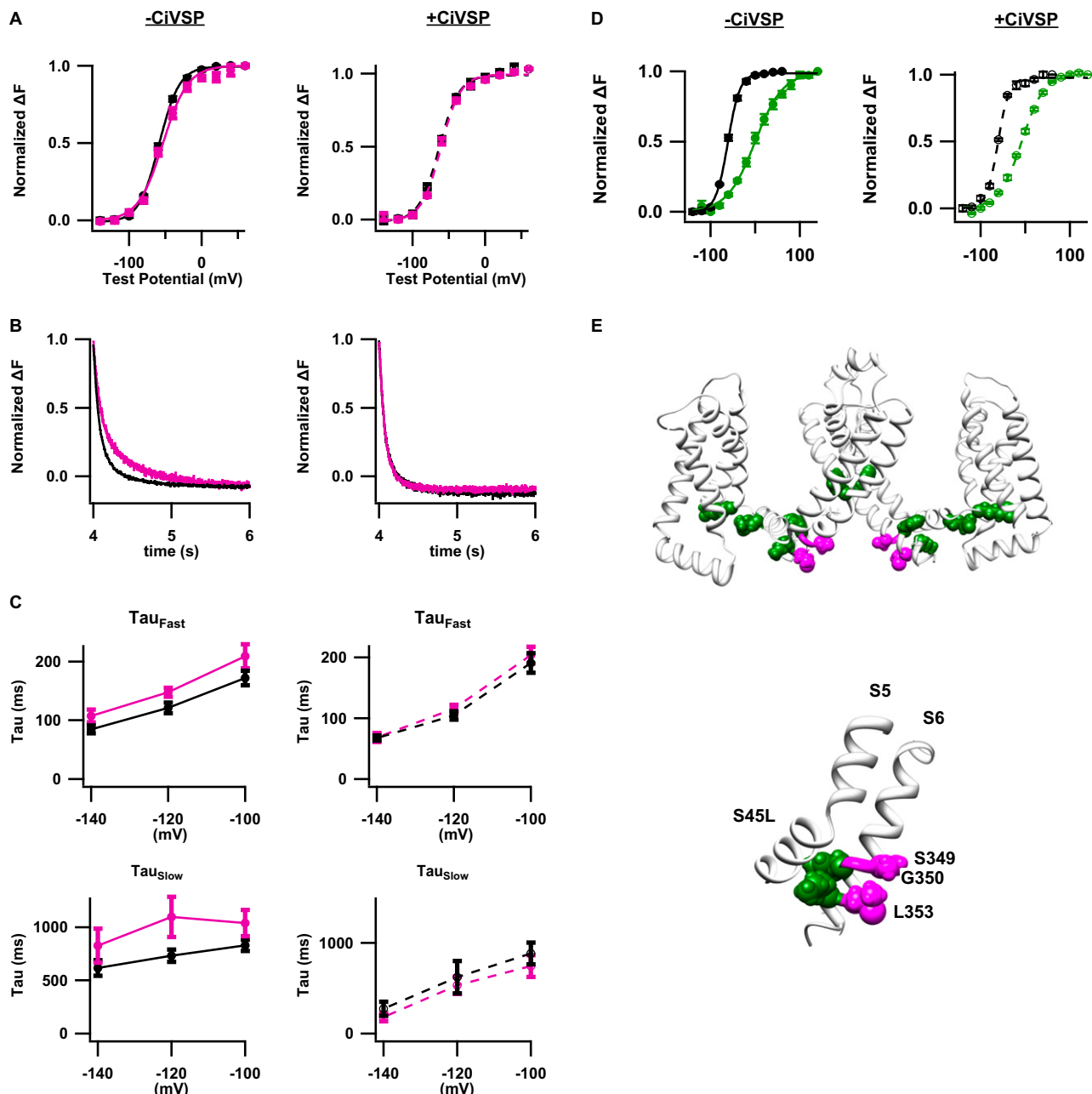
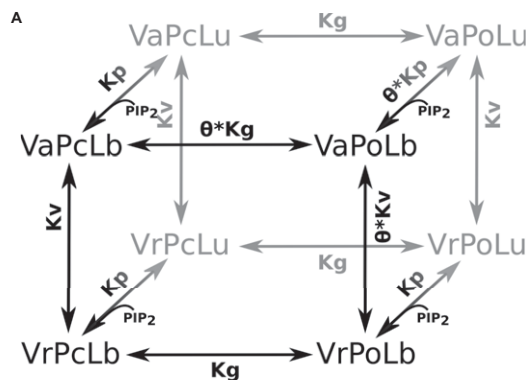


Fig. S5. The effects of mutation on VSD movements requires PIP₂ for residues in the S6 gate that are thought to be oriented into the channel pore. All mutations were made on the psWT Kv7.1 background. (A–C) A mutation (S349A) that affects VSD movements in the presence, but not in the absence, of PIP₂. Magenta and black indicate data from cells expressing S349A or psWT, respectively. Data from cells expressing channels alone or with CiVSP are shown to the Left and Right, respectively. F – V relationships in response to the voltage protocol in Fig. S4B (A), normalized ΔF upon a voltage step from +60 to −120 mV (B), and τ – V relations of deactivation (C). (D) An example of a mutation (F351A) that affects VSD movements in both the presence and the absence of PIP₂. Green and black indicate data from cells expressing F351A or psWT, respectively. Data from cells expressing channels alone or with CiVSP are shown to the Left and Right, respectively. F – V relationships for the deactivation protocol in Fig. S4B are shown. (E) Mapping of tested residues onto a Kv7.1 homology model (1). Magenta indicates the residues for which mutational effects on VSD movements are fully reversed by PIP₂ depletion, similar to L353K (Fig. 2) and S349A (A–C), and green indicates residues for which mutational effects on VSD movements persist even after PIP₂ depletion, similar to F351A (D).

1. Smith J, Vanoye CG, George AL, Jr., Meiler AL, Sanders CR (2007) Structural models for the KCNQ1 voltage-gated potassium channel. *Biochemistry* 46(49):14141–14152.



B	Kvo	z	Kg	Kp	Theta
psWT	45.12	1.86	0.02	0.75	8
psWT+CiVSP	45.12	1.86	0.02	0.01	8
L353K	45.12	1.86	1000	0.75	8
L353K+CiVSP	45.12	1.86	1000	0.01	8

Fig. S6. Model of Kv7.1 gating by voltage and PIP₂. (A) Full, balanced model scheme. The model consists of three particles: one VSD (*V*), one PD (*P*), and one lipid binding site (*L*). Each can assume two possible states: activated (*Va*) and resting (*Vr*), open (*Po*) and closed (*Pc*), PIP₂ bound (*Lb*) and unbound (*Lu*) for the VSD, PD, and lipid binding site, respectively. The activation of the VSD and the opening of the PD is dictated by the equilibrium constants *Kv* and *Kg*, respectively, in the absence of PIP₂. Where *Kv* = *P(Va)/P(Vr)* and *Kg* = *P(Po)/P(Pc)*, given that *L* = *Lu*. *Kp* is the equilibrium constant describing the binding of PIP₂ [*Kp* = *P(Lb)/P(Lu)*] when the VSD is resting or/and the PD is closed. The coupling factor, *θ*, represents the interactions between the particles that cause a relative stabilization of the VSD-activated, PD-open, and PIP₂-bound state. (B) Table of parameter values used to fit the experimental data.

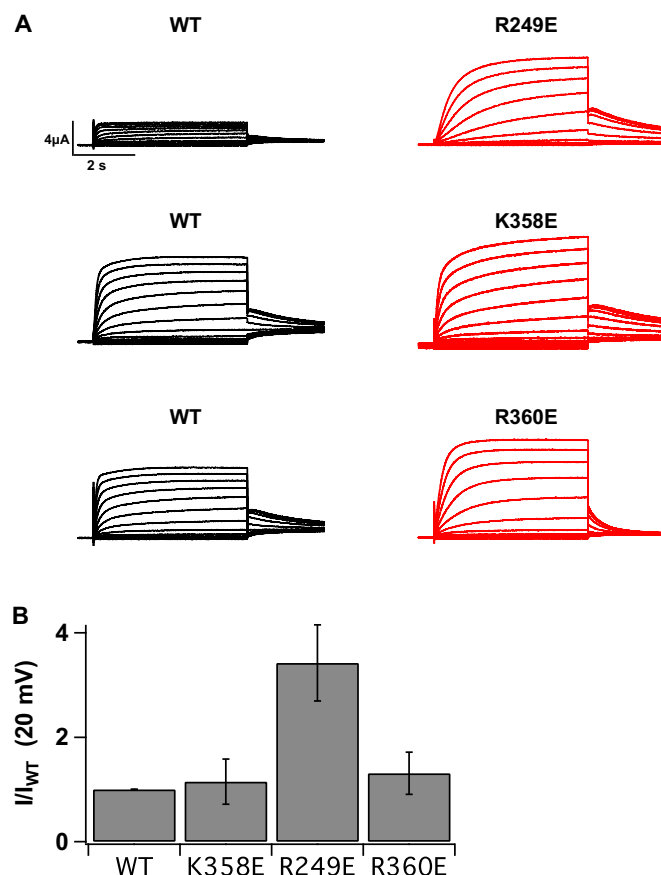


Fig. S7. Charge reversal mutations at the VSD–PD interface producing an increase in the whole-cell current. (A) Example currents from oocytes expressing mutant channels (Right, red) or wt channels (Left, black) recorded on the same day in response to voltage steps from -100 to +30 mV followed by a -40-mV tail. (B) Averaged current amplitude at +20 mV normalized to that of same-day WT control cells.

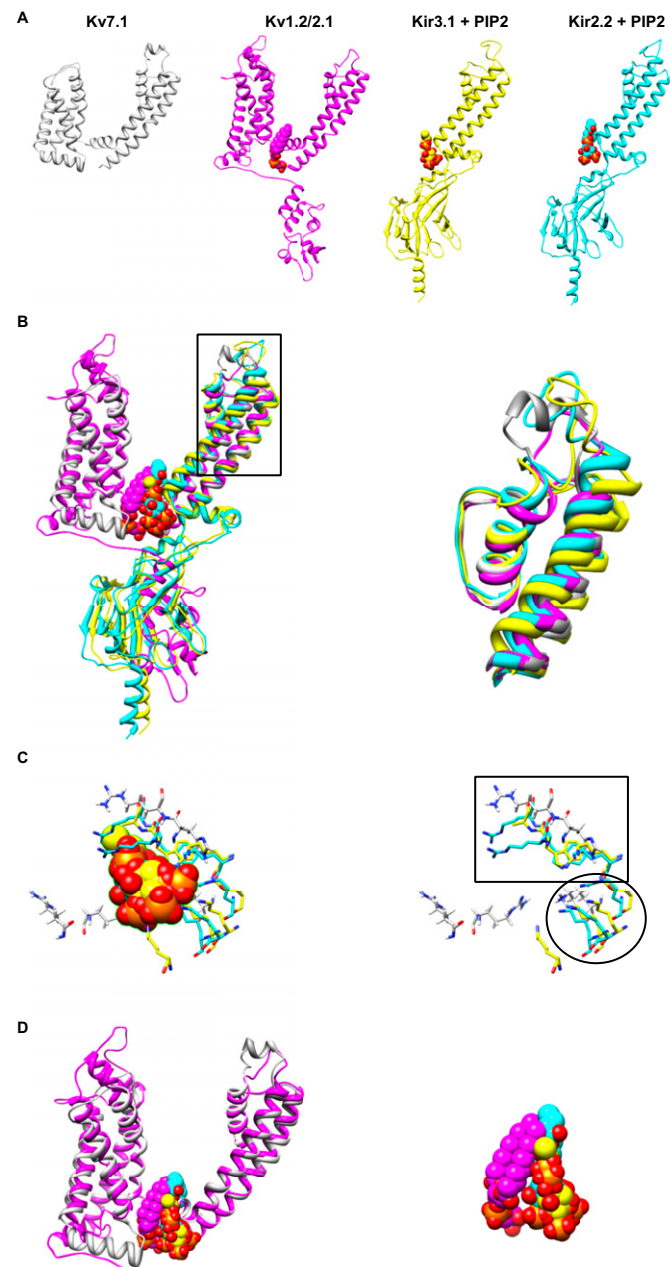


Fig. S8. Structural alignment of K⁺ channels demonstrates a conserved site for binding of anionic phospholipids. (A) Structures to be aligned: activated–open state Kv7.1 homology model (1), Kv1.2/2.1 crystal structure [magenta; Protein Data Bank (PDB) ID code 2R9R], Kir2.2 + PIP₂ crystal structure (cyan; PDB ID code 3SP1), Kir3.1 + PIP₂ crystal structure (yellow; PDB ID code 3SYO). (B) Alignment of the four structures in A using the Chimera matchmaker tool. Expanded view of the boxed region (Right) shows the excellent alignment of the conserved pore and filter structures. (C) View of the PIP₂ head groups of Kir2.2 and Kir3.1 (shown in sphere representation) with the important Kv7.1 residues, from this study, and the key Kir2.2 and Kir3.1 residues, identified crystallographically, for PIP₂ coordination shown in stick representation. The boxed cluster of residues includes residues in the Kv7.1 S4–S5 linker (H358, R259) and the Kir slide helix. The cluster of residues enclosed by the oval corresponds to residues in the Kv7.1 proximal C terminus (K354N) and in the Kir tether helix (C linker). Additional Kv7.1 C-terminal residues (R360, H363, R366) may contribute to this cluster, but are not resolved in the Kv7.1 homology model. (D) View of the Kv7.1 and Kv1.2/2.1 ribbons with an anionic phospholipid resolved in the Kv1.2/2.1 crystal structure and the PIP₂ molecules from Kir2.2 and Kir3.1 shown demonstrating the proximity of the anionic phospholipid in the Kv1.2/2.1 crystal structure to the putative PIP₂ binding site in Kv7.1, suggesting that anionic phospholipids (other than PIP₂) may play a role in the coupling of the VSD and PD in other Kv channels.

1. Smith J, Vanoye CG, George AL, Jr., Meiler AL, Sanders CR (2007) Structural models for the KCNQ1 voltage-gated potassium channel. *Biochemistry* 46(49):14141–14152.

Table S1. Table of long QT mutations expected to disrupt PIP₂-mediated coupling

Mutation	Location	Ref.
R190Q	S2–S3 linker	1
R190W	S2–S3 linker	2
H258N	S4–S5 linker	2
H258R	S4–S5 linker	2
R259H	S4–S5 linker	3
R259C	S4–S5 linker	4
R259L	S4–S5 linker	5
R360T	Proximal C terminus	2
R366Q	Proximal C terminus	6
R366W	Proximal C terminus	7
R366P	Proximal C terminus	8

- Chouabe C, et al. (2000) Novel mutations in KvLQT1 that affect I_{Ks} activation through interactions with I_{Sk}. *Cardiovasc Res* 45(4):971–980.
- Napolitano C, et al. (2005) Genetic testing in the long QT syndrome: Development and validation of an efficient approach to genotyping in clinical practice. *JAMA* 294(23):2975–2980.
- Millat G, et al. (2006) Spectrum of pathogenic mutations and associated polymorphisms in a cohort of 44 unrelated patients with long QT syndrome. *Clin Genet* 70(3):214–227.
- Kubota T, Shimizu W, Kamakura S, Horie M (2000) Hypokalemia-induced long QT syndrome with an underlying novel missense mutation in S4–S5 linker of KCNQ1. *J Cardiovasc Electrophysiol* 11(9):1048–1054.
- Choi G, et al. (2004) Spectrum and frequency of cardiac channel defects in swimming-triggered arrhythmia syndromes. *Circulation* 110(15):2119–2124.
- Splawski I, et al. (2000) Spectrum of mutations in long-QT syndrome genes. *KVLQT1*, *HERG*, *SCN5A*, *KCNE1*, and *KCNE2*. *Circulation* 102(10):1178–1185.
- Splawski I, et al. (1998) Genomic structure of three long QT syndrome genes: *KVLQT1*, *HERG*, and *KCNE1*. *Genomics* 51(1):86–97.
- Tanaka T, et al. (1997) Four novel *KVLQT1* and four novel *HERG* mutations in familial long-QT syndrome. *Circulation* 95(3):565–567.